JOURNAL OF MATERIALS SCIENCE 31 (1996) 4067–4076

Formation and characterization of the solid solutions $(Cr_xFe_{1-x})_2O_3$, $0 \leqslant x \leqslant 1$

S. MUSIĆ*, M. LENGLET†‡, S. POPOVIĆ*,§, B. HANNOYER†‡, I. CZAKÓ-NAGY¶, M. RISTIĆ*, D. BALZAR*, F. GASHI*

*Ruđer Bošković Institute, P.O. Box 1016, 10001 Zagreb, Croatia
†‡Laboratoire de Physicochimie des Materiaux, Universite de Rouen, IUT, BP 246, 76137 Mont-Saint-Aignan Cedex, France
§Department of Physics, Faculty of Sciences, P.O. Box 162, 10001 Zagreb, Croatia
¶Department of Nuclear Chemistry, Eötvös Loránd University, P.O. Box 32, 1518 Budapest, Hungary

The solid solutions $(Cr_xFe_{1-x})_2O_3$, $0 \leqslant x \leqslant 1$, were prepared by traditional ceramic procedures. The samples were characterized using X-ray diffraction, Mössbauer, Fourier transform infra-red (FT-IR) and optical spectroscopic measurements. In the whole concentration range two phases exist phase F, α-$(Cr_xFe_{1-x})_2O_3$, which is isostructural with α-Fe_2O_3 and phase C, which is closely related to Cr_2O_3. Phase F exists in samples heated up to 900 °C, for $0 \leqslant x \lesssim 0.95$. Phase C exists from $x \gtrsim 0.27$ to $x = 1$ for samples heated up to 900 °C and from $x \gtrsim 0.65$ to $x = 1$ for samples heated up to 1200 °C. For samples heated up to 900 °C, the solubility limits were 27.5 ± 0.5 mol % of Cr_2O_3 in α-Fe_2O_3 and 4.0 ± 0.5 mol % of α-Fe_2O_3 in Cr_2O_3. For the samples heated at 1200 °C the diffraction peaks for the F and C phases in the two phase region were severely overlapped and thus the solubility limits could not be determined accurately as for previous samples. ^{57}Fe Mössbauer spectra of the samples heated up to 1200 °C showed significant broadening of spectral lines and a gradual decrease of the hyperfine magnetic field with increase of x up to 0.50. For $x \gtrsim 0.7$, a paramagnetic doublet with collapsing sextet was observed. The spectra were interpreted in terms of an electronic relaxation effect; however, an agglomeration of iron ions which would contribute to the superparamagnetic effect could not be excluded. The FT-IR spectra showed transition effects in accordance with the X-ray diffraction results. The most intense absorption bands, observed for the samples heated up to 1200 °C, were located at ~460 and 370 nm (22 000 and 27 000 cm^{-1}) for $x \geqslant 0.5$, ~500 and 360 nm for $x < 0.3$, and might be correlated with the strong enhancement of the pair transitions through antiferromagnetic interactions. The intensification of the $^6A_1 \rightarrow 4T_1$ Fe^{3+} ions in all spectra and the development of the absorption at 13 000 cm^{-1} due to a metal-metal charge transfer ($Cr^{3+} \rightarrow Fe^{3+}$) transition, might be explained by exchange coupling which has been observed in some spinel compounds.

1. Introduction

Mixed metal oxides of aluminium, chromium, gallium and iron, having the corundum structure (space group $R\bar{3}c$, no. 167), have been the subject of many investigations from the academic standpoint and because of the practical importance of these compounds. They have found application in the production of technical ceramics, refractory materials, abrasives, and catalysts. Mixed metal oxides with the corundum structure are also important constituents of soils and sediments. The metal ions Fe^{3+}, Ga^{3+}, Cr^{3+} and Al^{3+} have similar ionic radii and therefore the lattice constants of their oxides are also similar. This fact favours the formation of solid solutions between themselves to form mixed oxides. At present, there are still discrepancies concerning the conditions of formation of the solid solutions and the properties of the corundum structured mixed metal oxides. It is reasonable to suppose that the discrepancies between the results of different authors in this field are mainly influenced by (a) the preparation procedure and (b) the technique applied for the sample characterization.

Recently, we initiated a systematic survey of the chemical and structural properties of mixed metal oxides having the corundum structure. We began by producing samples in the system Fe_2O_3–Ga_2O_3. These samples were prepared by chemical coprecipitation techniques with the hydroxide coprecipitates receiving a heat treatment at temperatures up to 600 °C [1]. The presence of only one phase, α-$(Fe_{1-x}Ga_x)_2O_3$, was observed for the compositions with $x = 0$ to $x \sim 0.95$. Lattice constants of the α-phase gradually decreased as x increased. For $x \gtrsim 0.95$, a mixture of α- and β-phases was present; the β-phase

0022–2461

being isostructural with monoclinic β-Ga_2O_3. The hyperfine magnetic structure, which was observed for α-$(Fe_{1-x}Ga_x)_2O_3$ at room temperature, collapsed for the composition with $x \approx 0.50$. The changes in the ^{57}Fe Mössbauer spectra of the α-$(Fe_{1-x}Ga_x)_2O_3$ phase were discussed in terms of the electronic relaxation and superparamagnetic effects.

The method of chemical coprecipitation was also used for the preparation of samples in the system Fe_2O_3–Cr_2O_3 [2]. The hydroxide coprecipitates, after heating up to 900 °C, converted to solid solutions α-$(Cr_xFe_{1-x})_2O_3$ at all concentrations. Lattice constants of the α-phase decreased as x increased; the main changes took place in the range $x \approx 0.3$–0.9. The samples having the initial fraction of Cr_2O_3 in the region from $x \approx 0.7$–0.8 showed the presence of two closely related phases. After an additional heat treatment at 1100 °C, the samples contained only the α-phase.

Structural properties of the system Al_2O_3–Cr_2O_3 were investigated across the whole concentration range [3]. The samples were prepared by mechanochemical activation of γ-AlOOH and Cr_2O_3 and the sintering of the resulting powder which was heated up to 1300 °C. The formation of solid solutions of the type $(Al_{1-x}Cr_x)_2O_3$ was observed in the whole concentration range. The replacement of Al^{3+} with Cr^{3+} resulted in a gradual increase of the lattice constants with x. For the molar fraction of Cr_2O_3, $x \gtrsim 0.5$, a phase closely related to Cr_2O_3 was found. The lattice constants of this phase increased with x, although the rate of increase was much smaller. Gradual changes in the FT-IR spectra were observed with increasing x.

The samples in the analogous system Al_2O_3–Fe_2O_3, prepared by the same experimental procedure [3], contained two types of solid solutions α-$(Al_xFe_{1-x})_2O_3$ [4]. For $0 \leqslant x \lesssim 0.9$, a phase closely related to α-Fe_2O_3 was found, whilst for $0.3 \lesssim x \leqslant 1$ a phase closely related to α-Al_2O_3 was present. In the two-phase region the lattice constants of both phases did not change while the fraction of the former phase decreased, and the fraction of the latter phase increased as x increased. On the other hand, in the single-phase regions the lattice constants of both phases decreased as x increased.

In the present work we have reinvestigated the properties of the mixed metal oxides formed in the system Fe_2O_3–Cr_2O_3, but using the solid state method for the preparation of the samples. The aim of this work was to ascertain structural differences between the samples in the system Fe_2O_3–Cr_2O_3, prepared by chemical coprecipitation [2], and the samples prepared by the solid state method. The formation of solid solutions was investigated by X-ray diffraction (XRD). Additional structural and physical properties of the system Fe_2O_3–Cr_2O_3 were investigated using ^{57}Fe Mössbauer, FT–IR and optical spectroscopy.

2. Experimental procedure

The metal oxides α-Fe_2O_3 and Cr_2O_3 (99.999%) were obtained from Ventron. The chemicals were dried to remove adsorbed water. The powders of these oxides in the correct stoichiometric ratios were mixed and mechanically activated using a planetary mill by Fritsch (pulverisette 5). An agate bowl and balls (99.9% SiO_2) were used. The mechanically activated powders were pressed into small rods, which were heated in air. The samples, in the series denoted as A were heated at 200 °C, 400 °C, 600 °C and 800 °C for 1 h at each temperature, and at 900 °C for 4 h, whilst the samples in series B were additionally heated at 1200 °C for 2 h. A standard laboratory furnace was used for heating the samples up to 900 °C, and a LKO II furnace with Kanthal heating elements was used to reach 1200 °C. The chemical composition of the samples and their notation are given in Table I.

TABLE I Chemical composition of the samples prepared in the system $(Cr_xFe_{1-x})_2O_3$.

Sample	Molar fraction	
	Cr_2O_3	Fe_2O_3
$S0_A$, $S0_B$	0	1
$S1_A$, $S1_B$	0.01	0.99
$S2_A$, $S2_B$	0.03	0.97
$S3_A$, $S3_B$	0.10	0.90
$S4_A$, $S4_B$	0.20	0.80
$S5_A$, $S5_B$	0.30	0.70
$S6_A$, $S6_B$	0.50	0.50
$S7_A$, $S7_B$	0.70	0.30
$S8_A$, $S8_B$	0.80	0.20
$S9_A$, $S9_B$	0.90	0.10
$S10_A$, $S10_B$	0.97	0.03
$S11_A$, $S11_B$	0.99	0.01
$S12_A$, $S12_B$	1	0

X-ray diffraction powder patterns were taken at room temperature (25 °C) using a Philips MPD 1880 diffractometer with monochromatized Cu$K\alpha$ radiation (graphite monochromator). The interplanar spacings of the studied samples were measured in relation to α-Al_2O_3 (corundum), used as an internal standard, with lattice constants at 25 °C (in terms of hexagonal axes): $a = 0.4758$, $c = 1.2991$ nm [5]. The diffraction pattern of a corundum-type oxide does not contain $0\,0\,l$ diffraction peaks at higher Bragg angles, which could be utilized in calculating the c lattice constant. Instead, one could make use of $h\,k\,l$ diffraction peaks for which the index l is dominant in relation to the indices h and k. The ionic radii of iron and chromium, having a sixfold coordination, are very similar: 0.065 nm for Fe^{3+} and 0.062 nm for Cr^{3+} [6]. The lattice constants of the oxides α-Fe_2O_3 (mineral name hematite) and Cr_2O_3 (eskolaite) measured in the present work and in previous work [2] were in excellent agreement with those given in the literature [5] at 25 °C (in terms of hexagonal axes): $a = 0.5034$, $c = 1.3752$ nm for α-Fe_2O_3, and $a = 0.4954$, $c = 1.3584$ nm for Cr_2O_3.

^{57}Fe Mössbauer spectra were recorded at the Eötvös-Loránd University in Budapest using a Wissel spectrometer. The measured spectra were fitted with the SIRIUS program [7]. ^{57}Fe Mössbauer spectra were also recorded at the University of Rouen.

FT-IR spectra were recorded at room temperature using a Perkin-Elmer spectrometer (model 1720x). The FT-IR spectrometer was coupled to a personal computer loaded with an IR Data Manager (IRDM) program. The samples were pressed into discs using spectroscopically pure KBr. A Perkin-Elmer FT-IR spectrometer (model 2000) was used for the measurements in the far infrared region. In this case, the samples in the form of powder were pressed into polyethylene foil.

Optical spectra were recorded at room temperature using a Perkin-Elmer lambda 9 spectrophotometer equipped with an integrating sphere attachment and a 7300 computer.

3. Results and discussion

3.1. X-ray diffraction

The results of X-ray diffraction phase analysis are given in Table II. In the whole concentration range two phases exist, phase F, α-$(Cr_xFe_{1-x})_2O_3$, which is isostructural with α-Fe_2O_3, and phase C, which is closely related to Cr_2O_3. A characteristic section of the diffraction patterns (recorded at 25 °C) for a sample with $x = 0.70$, heated up to 900 °C ($S7_A$) and up to 1200 °C ($S7_B$), are shown in Fig. 1. One can see an increase of the fraction of phase F and a decrease of the fraction of phase C with an increase in the temperature. Characteristic sections of the diffraction patterns (recorded at 25 °C) for samples, heated up to 1200 °C, with $x = 0$ ($S0_B$), 0.70 ($S7_B$) and 1 ($S12_B$), are shown in Fig. 2. One can notice a shift of the 214 and 300 diffraction peaks towards higher angles with the increase of the initial molar fraction of Cr_2O_3, x. The 214 and 300 diffraction peaks of α-Al_2O_3, used as an internal standard, are also shown in Fig. 2. The variation of the interplanar spacings $d(300)$ and $d(214)$ of both F and C phases, for the samples heated up to 900 °C and for the samples heated up to 1200 °C, as a function of the initial molar fraction of Cr_2O_3, x, is shown in Fig. 3. Vertical bars indicate the estimated experimental errors; at points where the bars are not shown, the error is of the size of marks shown in the figure or smaller.

TABLE II Phase composition of the samples in the system α-Fe_2O_3–Cr_2O_3 obtained by X-ray powder diffraction. Phase F: α-$(Cr_xFe_{1-x})_2O_3$ isostructural with α-Fe_2O_3; phase C: closely related to Cr_2O_3.

Molar fraction of Cr_2O_3, x	Phase composition (approximate molar fraction)	
	Samples heated up to 900 °C (A)	Samples heated up to 1200 °C (B)
0	α-Fe_2O_3	α-Fe_2O_3
0.01	F	F
0.03	F	F
0.10	F	F
0.20	F	F
0.30	F + C (< 0.05)	F
0.50	F + C (0.33)	F
0.70	C + F (0.38)	F + C (0.15)
0.80	C + F (0.23)	F + C (0.40)
0.90	C + F (0.10)	C + F (0.10)
0.97	C	C
0.99	C	C
1	Cr_2O_3	Cr_2O_3

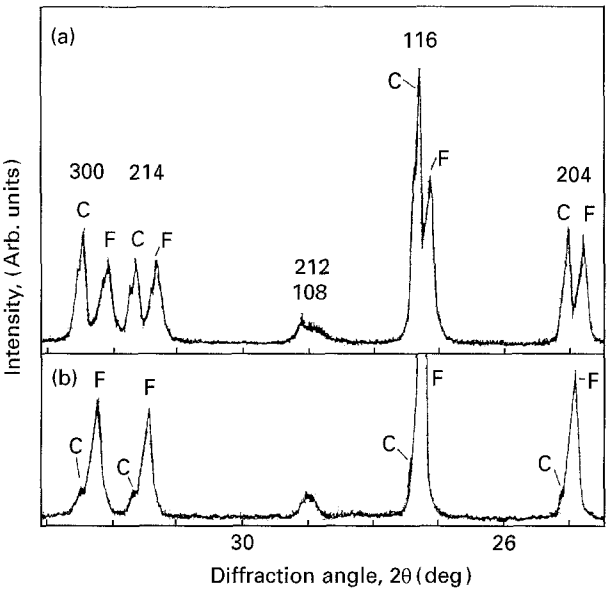

Figure 1 A section of the X-ray diffraction patterns (recorded at 25 °C) of (a) sample with $x = 0.70$, heated up to 900 °C ($S7_A$) and (b) up to 1200 °C ($S7_B$), showing the change in the phase concentrations of the F and C phases with temperature.

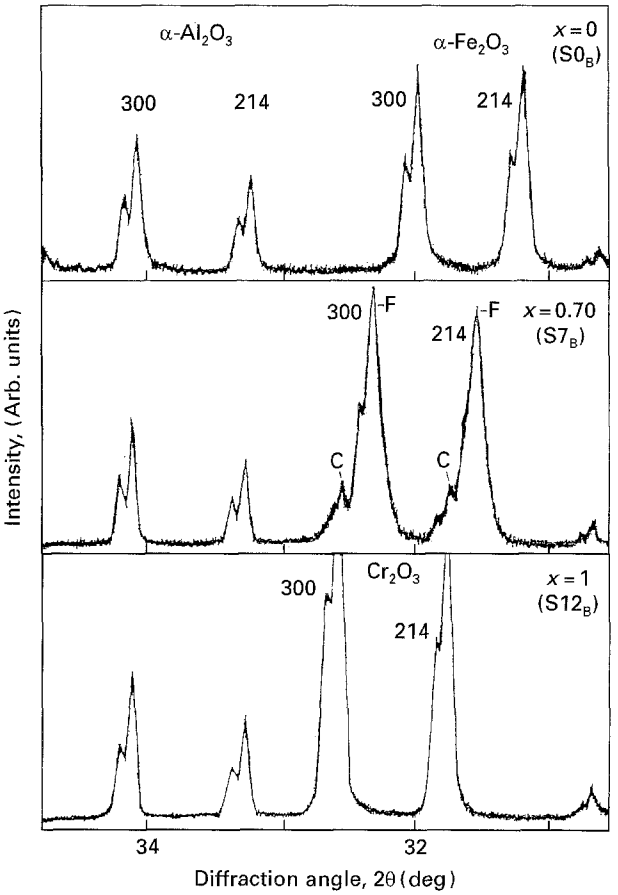

Figure 2 A section of the X-ray diffraction patterns (recorded at 25 °C) of samples heated up to 1200 °C, $S0_B$ ($x = 0$), $S7_B$ ($x = 0.70$) and $S12_B$ ($x = 1$), showing the shift of the 214 and 300 diffraction peaks with the value of x. The 214 and 300 diffraction peaks of α-Al_2O_3 used as an internal standard, are also shown.

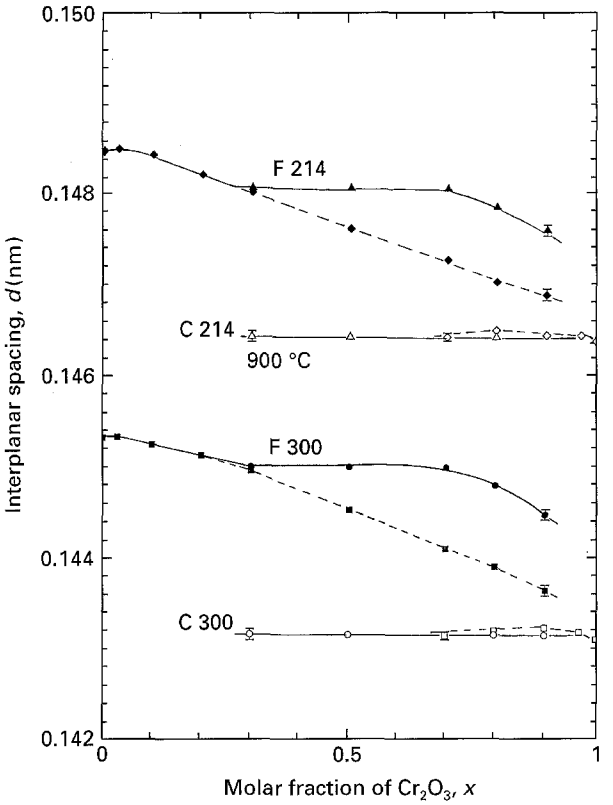

Figure 3 Variation of the interplanar spacings $d(300)$ and $d(214)$ of the F and C phases with the molar fraction of Cr_2O_3, x, for the samples heated up to 900 and 1200 °C. Vertical bars indicate an estimated experimental error. Descriptions: $d(300)$: phase F, (●) 900 °C, (■) 1200 °C; phase C, (○) 900 °C, □ 1200 °C; $d(214)$: phase F, (▲) 900 °C, (◆) 1200 °C; phase C, (△) 900 °C, (◇) 1200 °C.

The phase F exists in the range $0 \leqslant x \lesssim 0.95$. Its lattice constants gradually decrease as x increases, except for samples heated at 900 °C in the middle of the concentration range ($0.3 \lesssim x \lesssim 0.7$). The phase C exists from $x \gtrsim 0.27$ to $x = 1$ for samples heated at 900 °C, and from $x \gtrsim 0.65$ to $x = 1$ for the samples heated at 1200 °C. Its lattice constants only show a small variation with x, being about 0.03% larger than those of Cr_2O_3. Therefore, the two-phase region is much wider for samples heated at 900 °C than for samples heated at 1200 °C. For both groups of samples (A and B series) the fraction of phase F decreases, whilst the fraction of phase C increases as x increases.

For the samples heated at 900 °C the intensities of the prominent diffraction peaks for both F and C phases were plotted as a function of x. The extrapolation to zero intensity gave the following solubility limits: 27.5 ± 0.5 mol % of Cr_2O_3 in α-Fe_2O_3 and 4.0 ± 0.5 mol % of α-Fe_2O_3 in Cr_2O_3. For samples heated at 1200 °C the diffraction peaks for the F and C phases in the two-phase region were severely overlapped, and the solubility limits could not be determined as accurately as in the case of the samples heated at 900 °C.

The following comparison between samples prepared in the present work and those obtained by chemical coprecipitation [2] can be performed. The Bragg angles of diffraction peaks, and therefore the lattice constants of both the F and C phases of the present samples heated up to 1200 °C (series B) are very similar to the ones of samples obtained by chemical coprecipitation and heated up to 900 °C. The molar fractions of the F and C phases in the present samples heated up to 900 °C are very similar to those of samples obtained by chemical coprecipitation and heated up to the same temperature, although the two-phase region is broader in the former than in the latter case ($0.7 \lesssim x \lesssim 0.8$). The samples, obtained by chemical coprecipitation and heated up to 1100 °C [2], were single-phase solid solutions across the whole concentration range. These experiments clearly indicate that the formation of solid solutions in the system Fe_2O_3–Cr_2O_3, as evaluated by XRD was strongly dependent on the preparation procedure and the temperature of heating, and to a smaller extent on the time of heating.

Recently, Tsokov *et al.* [8] also used the chemical coprecipitation method to investigate the formation of solid solution in the system Fe_2O_3–Cr_2O_3. However, they concluded that the formation of solid solutions began at 500 °C. The mechanical pretreatment of hydroxide coprecipitates decreased the temperature of formation of the solid solutions to 350 °C. Busca *et al.* [9] characterized $Fe_{2-x}Cr_xO_3$ samples at $x = 0$, 0.66, 1, 1.33 and 2, that were prepared using the following steps: (a) chemical coprecipitation at pH 9, (b) ageing in the mother liquor at 60 °C for 2 days, (c) drying of the separated coprecipitate at 117 °C for 3 h, and (d) calcination of the mixed hydroxide at 400 °C for 5 h. The characterization of the precursor phase showed the presence of α-FeOOH (goethite) for $x = 0$, whilst with an increase of Cr content there was an increase of the amorphous phase, which was solely present in the sample for $x = 2$. After the calcination, the diffraction peaks of the solid solutions shifted toward lower d values with increasing Cr content, whilst the line positions for $x = 0$ and $x = 2$ corresponded to those of hematite and eskolaite, respectively.

3.2. Mössbauer spectroscopy

The structural changes in the samples $(Cr_xFe_{1-x})_2O_3$, $0 \leqslant x \leqslant 1$, observed by XRD, were reflected in the Mössbauer effect in these samples. Figs 4 and 5 show the Mössbauer spectra of selected samples from series B, recorded at room temperature. These spectra were recorded at the Eötvös-Loránd University in Budapest. ^{57}Fe Mössbauer parameters calculated on the basis of these spectra and those recorded at the University of Rouen are given in Tables III and IV, respectively. The Mössbauer spectrum for sample SO_B was typical for α-Fe_2O_3. Fig. 4 shows a significant broadening of spectral lines and a gradual decrease of the hyperfine magnetic field (Tables III and IV) with an increase in x up to 0.50.

It is generally understood that the substitution of Fe^{3+} ions with certain metal cations in α-Fe_2O_3 can decrease the hyperfine magnetic field value. For instance, this effect was observed [10] in the early stage of formation of $NiFe_2O_4$ by thermal decomposition of a mixture of nitrate salts of Ni^{2+} and Fe^{3+}. Two relatively well resolved sextets, M_1 and M_2, were ascribed to α-Fe_2O_3 with dissolved Ni^{2+} ions. In this case the hyperfine magnetic field M_1 increased from

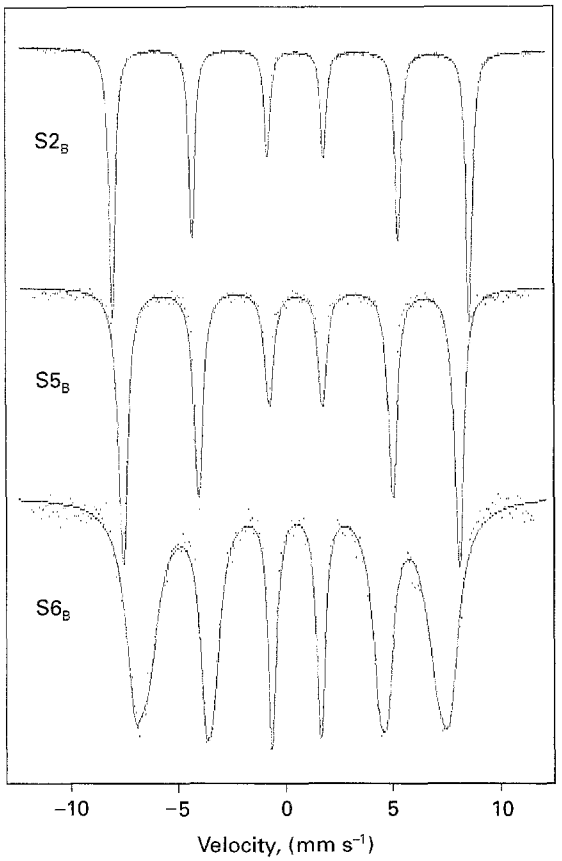

Figure 4 ^{57}Fe Mössbauer spectra of samples $S2_B$ ($x = 0.03$), $S5_B$ ($x = 0.30$) and $S6_B$ ($x = 0.50$), recorded at room temperature.

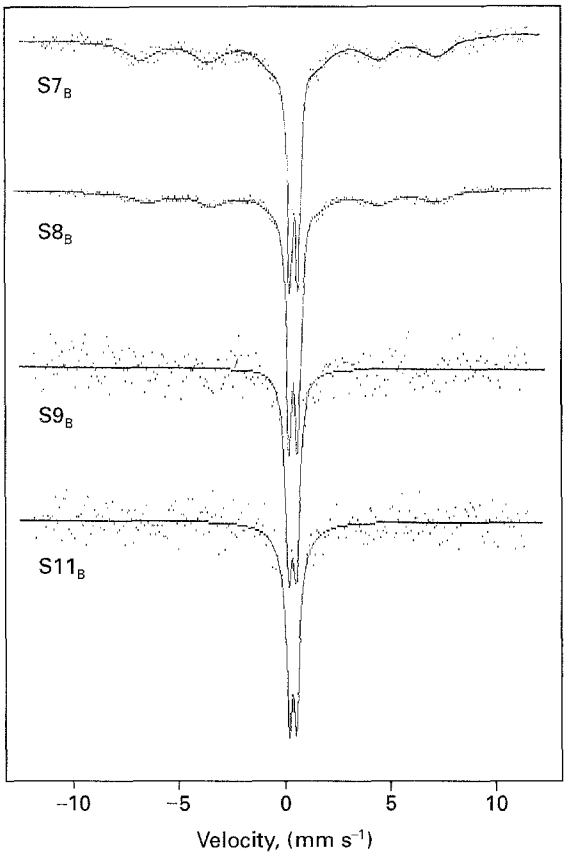

Figure 5 ^{57}Fe Mössbauer spectra of samples $S7_B$ ($x = 0.70$), $S8_B$ ($x = 0.80$), $S9_B$ ($x = 0.90$) and $S11_B$ ($x = 0.99$), recorded at room temperature.

37 482 to 41 142 kA m^{-1} for the samples heated between 200–400 °C, whilst the hyperfine magnetic field M_2 increased from 34 935 to 39 869 kA m^{-1} for the samples heated between 200–300 °C.

The spectrum of sample $S6_B$ ($x = 0.50$), shown in Fig. 4, indicates the hyperfine fields distribution. This spectrum was fitted as the superposition of two sextets, which in the present case does not imply the existence of two distinctly separated oxide phases. As already discussed, the X-ray diffraction measurements showed only F-type solid solution in the sample $S6_B$. For $x \gtrsim 0.7$, a paramagnetic doublet with a collapsing sextet is observed. The spectrum of sample $S11_B$ ($x = 0.99$) showed only a paramagnetic doublet (Fig. 5). The fitting procedure for the spectrum of sample $S11_B$ was improved by introducing an additional broad singlet with a small relative intensity. The collapsing of the hyperfine magnetic field and the broadening of spectral lines with an increase of x was numerically evaluated using a fitting procedure which takes to account the hyperfine fields distribution (Table IV).

In previous work [2], the Mössbauer spectra of the samples in the system $(1 - x)Fe_2O_3 + xCr_2O_3$ also indicated a decrease in the hyperfine magnetic field and a broadening of the spectral lines with an increase of x. However, the existence of magnetic split spectra were shifted to higher x values, than is shown in the present case. For instance, two relatively well separated sextets were observed in the room temperature spectrum for $x = 0.70$. Mössbauer spectroscopy also confirmed the fact established by X-ray diffraction, i.e., the behaviour of the solid solutions formed in α-$(Cr_xFe_{1-x})_2O_3$ was dependent on the preparation procedure and the temperature of heating, and not only on the x value.

Volenik and Seberini [11] recorded Mössbauer spectra of the mixed oxides $Fe_{2-y}Cr_yO_3$, $y = 0$, 0.29, 0.61, 0.96, 1.33 and 1.64. At room temperature, a hyperfine magnetic field was observed up to $y = 0.96$, whilst for $y = 1.33$ and 1.64 the Mössbauer spectra consisted of only paramagnetic doublets. Mössbauer spectroscopy was also used to investigate the effect of annealing on the spectra of Cr_2O_3–3.85 wt % Fe_2O_3 [12, 13]. In the first paper [12], it was assumed that the annealing at 1400 °C caused a uniform distribution of Fe^{3+} ions in the host matrix, which was not the case at 1250 °C. In their second paper [13], the authors suggested that an annealing temperature of 1250 °C was sufficient to cause a uniform distribution of the Fe^{3+} ions in the Cr_2O_3 host. However, slow cooling of the solid solution to room temperature caused clustering of the Fe^{3+} ions.

The Cr^{3+} ions incorporated into the α-Fe_2O_3 structure are statistically distributed, whilst at the Cr_2O_3-rich side the same argument is valid for the Fe^{3+} ions. At a certain concentration of Cr^{3+} and Fe^{3+} a separation of solid solutions is possible, as observed in the present work. In these mixed oxides various lattice defects can also exist as a consequence of the preparation procedure. Due to these phenomena, ^{57}Fe resonant atoms have different types of nearest-neighbour configurations, i.e., a different electronic environment, and consequently, ^{57}Fe resonant

TABLE III ^{57}Fe Mössbauer parameters of the B series samples, calculated on the basis of the spectra recorded at room temperature at the Eötvös-Loránd University in Budapest.

Sample	δ isomer shift relative to α-Fe ($mm\ s^{-1}$)	ΔE_q quadrupole splitting of the sextet ($mm\ s^{-1}$)	Δ quadrupole doublet ($mm\ s^{-1}$)	H hyperfine magnetic field ($kA\ m^{-1}$)	Γ line width ($mm\ s^{-1}$)
$S2_B$	0.389	− 0.214		41063	0.305
$S3_B$	0.393	− 0.218		40745	0.331
$S4_B$	0.390	− 0.217		40029	0.390
$S5_B$	0.387	− 0.217		39153	0.484
$S6_B$	0.389	− 0.050		36289	1.004 ($L^*_{1,6}$) 0.576 ($L_{2,5}$) 0.353 ($L_{3,4}$)
	0.385	− 0.041		33424	1.299 ($L_{1,6}$) 0.930 ($L_{2,5}$) 0.539 ($L_{3,4}$)
$S7_B$	0.381		0.396		0.311
	0.302	− 0.226		34697	1.617
$S8_B$	0.378		0.376		0.314
	0.389	− 0.172		32867	1.490
$S9_B$	0.373		0.348		0.380
$S10_B$	0.367		0.333		0.312
$S11_B$	0.354				1.228
	0.377		0.313		0.258

* L = spectral line.

TABLE IV ^{57}Fe Mössbauer parameters of the B series samples, calculated on the basis of the spectra recorded at the University of Rouen.

Sample	δ_{Fe} ($mm\ s^{-1}$)	Δ_{Eq} ($mm\ s^{-1}$)	Δ ($mm\ s^{-1}$)	H $kA\ m^{-1}$	1/2Γ ($mm\ s^{-1}$)	H^{**}_{ave} $kA\ m^{-1}$	$p(H_{hf})$** $kA\ m^{-1}$	1/2Γ** ($mm\ s^{-1}$)
$S0_B$	0.372	− 0.182		41382	0.134			
$S1_B$	0.374	− 0.198		41334	0.133			
$S2_B$	0.373	− 0.210		41230	0.136			
$S3_B$	0.371	− 0.220		40856	0.152			
$S4_B$	0.372	− 0.216		40228	0.178	40140	795.8	0.122
$S5_B$	0.372	− 0.212		39265	0.224	38970	795.8	0.143
$S6_B$	0.369	− 0.205				34180	795.8	0.128
$S7_B$	0.359		0.382		0.151			
	0.367	− 0.158				16386	795.8	0.169
$S8_B$	0.355		0.357		0.145			
	0.317	− 0.237				10775	1591.6	0.166
$S9_B$	0.355		0.345		0.157			
	0.317	− 0.239				9056	1591.6	0.183

* Mössbauer spectra were recorded at room temperature.
** Fit with hyperfine field distribution.

atoms are characterized by different contributions to the Mössbauer effect. The corresponding Mössbauer spectra of α-$(Cr_xFe_{1-x})_2O_3$ and similar oxide systems show a distribution of hyperfine magnetic fields, i.e., the electronic relaxation. However, for larger values of x the superparamagnetic effect can also be present. This means that there is some kind of agglomeration of ^{57}Fe resonant atoms in the Cr_2O_3 matrix, and that these agglomerates behave magnetically in the same way as superfine iron oxide particles.

3.3. FT-IR spectroscopy

The characteristic results of the FT-IR spectroscopic measurements, for the samples from series A and B, are summarized in Figs 6 and 7, respectively. The FT-IR spectrum of sample $S0_A$ (α-Fe_2O_3) is characterized with a very strong band at 564 cm^{-1}, a strong band at 481 cm^{-1}, a weak band at 384 cm^{-1} and shoulders at 619 and 439 cm^{-1}. With an increase of x up to 0.20 (sample $S4_A$) gradual shifts of the IR bands, 564 → 579 and 481 → 504 cm^{-1}, are observed. More distinct changes in the FT-IR spectra are

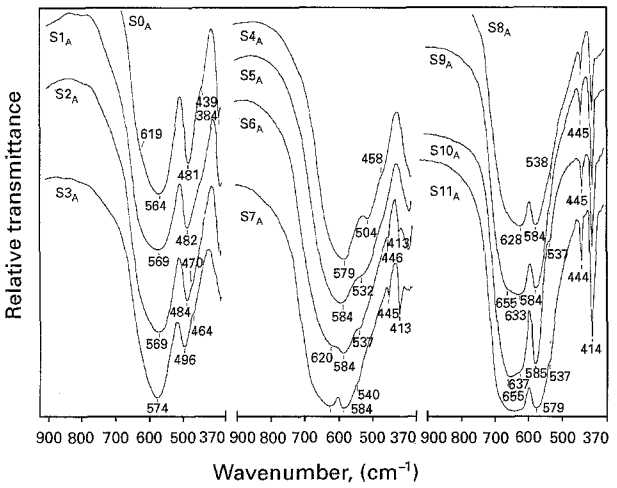

Figure 6 Fourier transform IR spectra of the samples from series A (samples $S0_A$ to $S11_A$), recorded at room temperature.

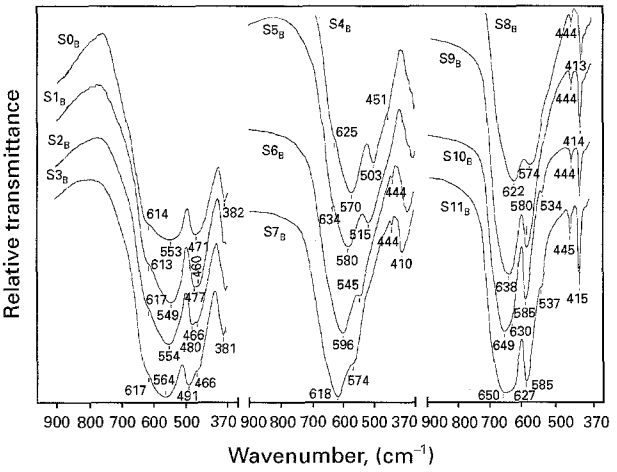

Figure 7 Fourier transform IR spectra of the samples from series B (samples $S0_B$ to $S11_B$), recorded at room temperature.

observed for $x = 0.30$ (sample $S5_A$) and $x = 0.50$ (sample $S6_A$). In the FT-IR spectrum of sample $S5_A$ a very broad band with a transmittance minimum at 584 cm^{-1} and a shoulder at 532 cm^{-1} are observed. The FT-IR spectrum of sample $S6_A$ consists of IR bands which are characteristic of the C phase, i.e., the band at 584 cm^{-1} with pronounced shoulders at 620 and 537 cm^{-1}, and weak bands at 446 and 413 cm^{-1}. With a further increase of x up to 1 there is a gradual formation of the spectrum corresponding to Cr_2O_3 (sample $S12_A$).

The FT-IR spectra of the samples from series B (heated up to 1200 °C) showed similar changes (Fig. 7). The main feature of the α-Fe_2O_3 spectrum is better preserved (up to $x = 0.30$) than in the case of the samples from series A. Weak IR bands at 444 cm^{-1} and 410 cm^{-1} are observed in the spectrum for $x = 0.50$ (sample $S6_B$). The characteristic IR bands of the C phase at 444 and 413 cm^{-1} are clearly visible in the spectrum of sample $S8_B$ ($x = 0.80$). This is in accordance with the XRD results which showed a significant increase of the fraction of C phase in the sample with $x = 0.80$. Generally, changes observed in the FT-IR spectra of the samples from series B, corresponding to the transition α-$Fe_2O_3 \rightarrow Cr_2O_3$, were shifted to higher x-values in relation to the samples from series A. This is in accordance with XRD results which showed dominance of the F phase, in the samples from B series, in a wider range of x-values.

Vibrational spectroscopy has also been used by other researchers to characterize solid solutions in the system α-Fe_2O_3–Cr_2O_3. For instance, Gillot *et al.* [14] found linear shifts of IR bands to greater wave numbers in the system α-$(Fe_{6-y}Cr_y)O_9$, $0 \leqslant y \leqslant 4$. The extrapolations of the IR band positions to $y = 6$ gave values of the IR bands of 639, 582 and 440 cm^{-1}, which are characteristic of Cr_2O_3. McCarty and Boehme [15] used X-ray diffraction and Raman spectroscopy to characterize the system $Fe_{2-y}Cr_yO_3$, $0 \leqslant y \leqslant 2$. The authors concluded that a single solid solution was formed over the whole concentration range despite the fact that their samples were prepared in similar manner to our samples.

3.4. Optical spectroscopy

The optical spectra were recorded for the end-members α-Fe_2O_3 and Cr_2O_3, as well as for the solid solutions α-$(Cr_xFe_{1-x})_2O_3$, $0 \leqslant x \leqslant 1$, from series B (Figs 8–12, Tables V–VII).

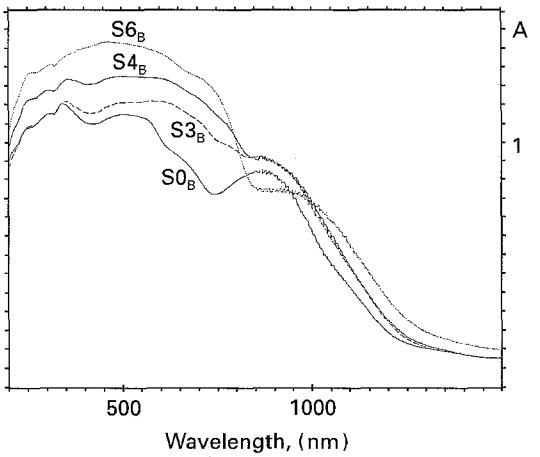

Figure 8 Diffuse reflectance spectra of $(Cr_xFe_{1-x})_2O_3$ solid solutions (series B). Descriptions: $S0_B$ ($x = 0$), $S3_B$ ($x = 0.10$), $S4_B$ ($x = 0.20$) and $S6_B$ ($x = 0.50$).

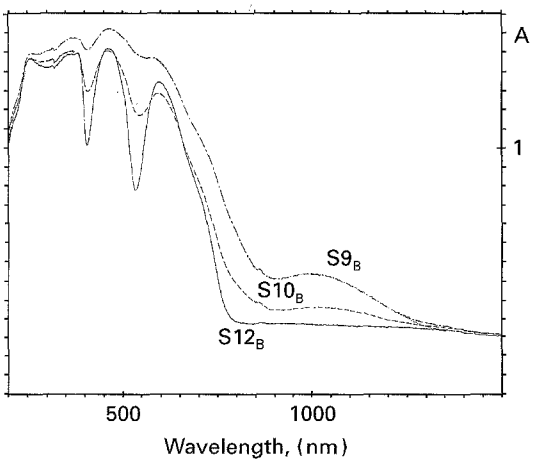

Figure 9 Diffuse reflectance-spectra of $(Cr_xFe_{1-x})_2O_3$ solid solutions. Descriptions: $S9_B$ ($x = 0.90$), $S10_B$ ($x = 0.97$) and $S12_B$ ($x = 1$).

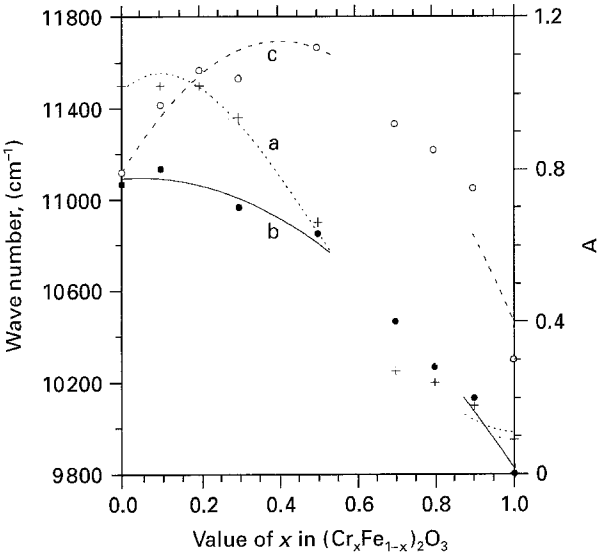

Figure 10 Analysis of the Fe^{3+} diffuse reflectance spectrum as a function of x in $(Cr_xFe_{1-x})_2O_3$ solid solutions (series B). Descriptions: (+) a: $^6A_1 \rightarrow {}^4T_1$ position; b: $I_{^6A_1} \rightarrow {}^4T_1$ (Fe^{3+}); (○) c: I_{13000}.

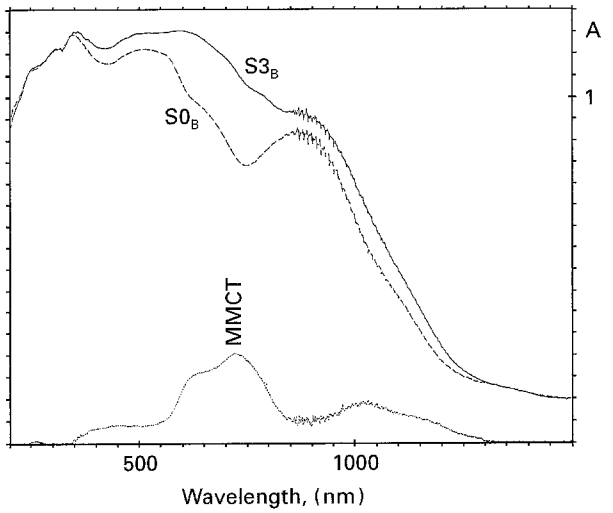

Figure 11 Diffuse reflectance spectra of $(Cr_{0.1}Fe_{0.9})_2O_3$ (sample $S3_B$) and α-Fe_2O_3 (sample $S0_B$) and the difference spectrum (MMCT).

Three types of electronic transitions occur in the optical spectrum of α-Fe_2O_3 (Table V): (a) Fe^{3+} ligand field transitions, (b) pair transitions which result from the simultaneous excitation of two magnetically-coupled Fe^{3+} ions which occupy adjacent sites, and (c) ligand to metal charge-transfer transitions ($O^{2-} \rightarrow Fe^{3+}$), LMCT.

In principle, all of the transitions from the ground state $^6A_1$ (^6S) to the excited ligand field states are both spin and parity-forbidden. In iron oxides and ferrites, these transitions become allowed through the magnetic coupling of electronic spins of next-nearest neighbour Fe^{3+} ions in the crystal structure. An additional phenomenon resulting from the magnetic coupling of adjacent Fe^{3+} ions is the presence of new absorption features corresponding to the simultaneous excitation of two Fe^{3+} centres. These features occur at energies given approximately by the sum of two single ion Fe^{3+} ligand field transitions (several absorption bands in the spectrum of Fe^{3+} cations in

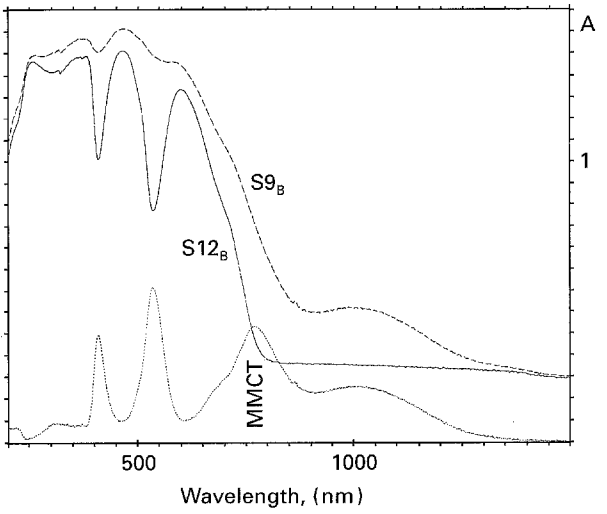

Figure 12 Diffuse reflectance spectra of $(Cr_{0.9}Fe_{0.1})_2O_3$ (sample $S9_B$) and Cr_2O_3 (sample $S12_B$) and the difference spectrum (MMCT).

Al_2O_3 have been demonstrated to result from these Fe^{3+}–Fe^{3+} pair excitation [18]).

In α-Fe_2O_3, the pair transitions $^6A_1 + {}^6A_1 \rightarrow {}^4T_1 + {}^4T_1$ at 510 nm (19 600 cm^{-1}) and $^6A_1 + {}^6A_1 \rightarrow {}^4T_2 + {}^4T_2$ near 340 nm (29 400 cm^{-1}) are more intense than those of the other iron oxides and oxyhydroxide minerals. The minerals having FeO_6 coordination polyhedra in edge and corner-sharing arrangements allow relatively strong magnetic coupling via superexchange interactions. In α-Fe_2O_3, however, FeO_6 polyhedra are also in face-sharing arrangements. The face-sharing arrangement results in a trigonal distortion of the FeO_6 coordination polyhedra. Molecular orbital calculations show that the trigonal distortion increases the spin-polarization of the oxygen bridging face-sharing FeO_6 polyhedra. This implies that the superexchange interactions, and hence the strength of the magnetic coupling between face-sharing FeO_6 polyhedra in α-Fe_2O_3, will be greater than that between the edge-sharing FeO_6 polyhedra in the other oxides and oxyhydroxides [18].

The band at 305 nm (33 000 cm^{-1}) may be a composite of two transitions: the d–d transition $^6A_1 \rightarrow {}^4T_1({}^4P)$ and the pair transition $^6A_1 + {}^6A_1 \rightarrow {}^4E_1 + {}^4A_1 + {}^4T_1$ (G). The first LMCT transition is observed in the range 255–260 nm (in ferrites this transition is found at 38 000–40 000 cm^{-1}).

The spectrum of Cr_2O_3 has been treated as cubic, neglecting the small trigonal component (three oxygen ligands at 0.197 nm and three others at 0.202 nm). In agreement with the observed antiferromagnetism of Cr_2O_3 ($T_N = 307$ K, 34 °C), the intense bands observed in the range 360–380 nm (26 500–28 000 cm^{-1}) may be assigned to pair transitions: $^4A_{2g} + {}^4A_{2g} \rightarrow {}^2E_g + {}^2E_g$, $^2T_{1g} + {}^2T_{1g}$; the quartet–doublet are respectively found at 13 700 and 14 200 cm^{-1}. The intense absorption between 26 000–40 000 cm^{-1} includes the pair transitions, the $^4A_{2g} \rightarrow {}^4T_{1g}$ (P) transition (calculated wavenumber 35 000 cm^{-1}) and the first ligand metal charge transfer transition at 39 000–40 000 cm^{-1} (Table VI).

TABLE V Wavenumbers (cm^{-1}) and assignment of bands observed in the Fe_2O_3 optical spectrum.

Transition	Observed (calculated) transition wavenumbers (cm^{-1})			
$^6A_1 \rightarrow {}^4T_1(^4G)$	11 500	(11 500)	11 300	11 600
$^6A_1 \rightarrow {}^4T_2(^4G)$	15 400	(15 400)	15 400	
$2(^6A_1) \rightarrow 2(^4T_1)$	19 600		18 900	
$^6A_1 \rightarrow {}^4E_1{}^4A_1(^4G)$	~21 500	(22 450)	22 500	23 800
$^6A_1 \rightarrow {}^4T_2(^4D)$	~24 000	(24 000)	24 700	
$^6A_1 \rightarrow {}^4E(^4D)$		(26 100)	26 300	26 700
$2^6A_1 \rightarrow 2(^4T_2)$	29 400			
$^6A_1 \rightarrow {}^4T_1(^4P)$	~33 000	(34 000)	31 300	31 800
LMCT	39 500		37 000	38 900
Ligand field parameters				
$10D_q$	13 900		14 000	15 900
B	520		540	410
C	3450		3410	3930
Ref.	This work		[16]	[17]

Underlined bands are the maximum intensity bands of the spectrum.

TABLE VI Wavenumbers (cm^{-1}) and assignment of bands observed in Cr_2O_3 optical spectrum.

$^4A_{2g} \rightarrow {}^2E_g$	$^2T_{1g}$	$^4T_{2g}$	$^2T_{2g}$	$^4T_{1g}$ (F)	Pair transitions*	$^4T_{1g}$(P)	LMCT	Ligand field parameters (cm^{-1}) $10D_q$	B	Ref.
13 700	14 200	16 600	19 600	21 700				16600	480	[20]
								16600	480	[21]
13 700	14 100	16 500	19 700	21 800				16500	480	[22]
13 700	14 100	16 500	19 700	21 800	26 500–28 000	(35 000)	39 200			This work

* $2^4A_{2g} \rightarrow 2(^2E_g)$ and 2^2T_{1g}.

TABLE VII Analysis of the optical spectra of $(Cr_xFe_{1-x})_2O_3$ solid solutions.

Molar fraction of Cr_2O_3, x	Position (nm) and assignment of observed bands									
1			710*		595		462	360–380		255
0.97	1020		710*		592		460	365		260
0.90	990		~700*		~595		465	370		260
0.50	920		~700**				462			260
0.30	880		700**			480		375	310	265
0.20	870	780	700**		600			360	310	260
0.10	870	780	700**		600	(495)	470	350	310	255
0	870			650		510		342	305	255
Assignment										
Fe^{3+} Cr^{3+}	$^6A_1 \rightarrow {}^4A_{2g}$	$^4T_1$	^2E_g, $^2T_{1g}^*$ (MMCT)** Fe^{3+}–Cr^{3+}		$^4T_2$	$^4T_{2g}$ Fe^{3+} pair trans.	$^4T_{1g}$	Cr^{3+} and Fe^{3+} pair trans.	$^4T_1$(P)	LMCT

Underlined bands are the highest intensity bands of the spectrum.

The diffuse reflectance spectra of the $(Cr_xFe_{1-x})_2O_3$ solid solutions are shown in Figs 8 and 9. Most of the spectroscopic results are summarized in Table VII. The most intense absorption bands are located at ~460 and 370 nm (22 000 and 27 000 cm^{-1}) for $x \geqslant 0.5$, ~500 and 360 nm for $x \leqslant 0.3$ and may be correlated with the strong enhancement of the pair transitions through the antiferromagnetic interactions. The intensification of the $^6A_1 \rightarrow {}^4T_1$ Fe^{3+} ions in all spectra (Fig. 10, curve b) and the development of the absorption at 780 nm (13 000 cm^{-1}), which may be interpreted as a metal to metal charge transfer (MMCT) (Cr^{3+}–Fe^{3+}) transition, can be explained by exchange coupling observed in some spinel compounds, for instance, $ZnCr_{2-x}Fe_xO_4$; $Li_{0.5}(FeCr_x)\,Ga_{2.5-x}O_4$, and $Li_{0.5}Fe_{2.5-x}Cr_xO_4$ [23] (Fig. 10, curve c; Figs 11 and 12).

In many optical absorption spectra, in which intervalence charge transfer effects are observed, there is a distinct intensification of spin-allowed or

spin-forbidden bands in the near infra red (NIR) and visible regions. For oxides and silicates containing iron in both 2 + and 3 + oxidation states, in which intervalence charge transfer (IVCT) effects are observed, there is a distinct intensification of the spin-allowed Fe^{2+} bands in the NIR [24–26]. Self consistent field-X_α-(SCF-Xα-SW) molecular orbital calculations have been performed for several mixed valence, $(Fe_2O_{10})^{15-}$, clusters corresponding to edge sharing Fe^{2+} and Fe^{3+} coordination polyhedra. Absorption bands in the NIR and visible regions that are assigned to optically induced $Fe^{2+} \rightarrow Fe^{3+}$ charge transfer correspond to the $16a_1 \rightarrow 17a_1$ transition polarized along the metal–metal intermolecular distance. In these mixed valence iron compounds some absorption bands assigned to $Fe^{2+} \rightarrow Fe^{3+}$ charge transfer may in fact arise from a different electronic transition. In particular, magnetic coupling between adjacent Fe^{2+} and Fe^{3+} cations may result in intensification of spin-forbidden Fe^{2+} and Fe^{3+} ligand field transitions [27].

The influence of a strong antiferromagnetic coupling on the electronic spectrum of iron doped nickel gallates containing Fe^{3+} and Ni^{2+} cations octahedrally coordinated has been experimentally studied. The cluster $(FeNi)O_{15}^{10-}$ is characterized by a strong intensification of iron pair excitations and nickel spin-forbidden transitions and by the growth of a large electronic transition assigned to $Ni^{2+} + Fe^{3+} \rightarrow Ni^{3+} + Fe^{2+}$ intervalence charge transfer at 23 000 cm^{-1} [28].

Many attempts have been made to correlate the geometry and symmetry of the Cr^{3+} site in mixed crystals with the observed ligand field parameters in a point charge or related approach [29, 30] or to establish relations between $10D_q$ and the Cr–O distances. It is not possible to obtain exact data about the Cr–O distances in Cr^{3+} doped compounds by conventional X-ray or neutron diffraction methods without certain assumptions. Nevertheless, the evolution of the position of $^6A_1 \rightarrow {}^4T_1$ Fe^{3+} transition (Fig. 10, curve a) allows similar conclusions. Assuming the Racah parameters B and C constant, the variation of the energy of the $^6A_1 \rightarrow {}^4T_1$ transition as a function of increasing values of x would be consistent with increasing values of $10D_q$ corresponding to shorter Fe–O distances.

The spectrum of hematite recorded at 77 K (− 196 °C) reveals a better resolution of the transition of the ground state to the first possible excited state configuration $(t_{2g}^{\alpha})^3$ $(e_g^{\alpha})^1$ $(t_{2g}^{\beta})^1$ which gives the $^4T_1$ (^4G) and $^4T_2$(^4G) states. These transitions are observed at 865 nm (11 560 cm^{-1}) and 635 nm (15 750 cm^{-1}). The value 540 nm of the Racah parameter B deduced from these data is in agreement with that determined at room temperature (Table V). In the range 18 000–35 000 cm^{-1}, the remaining bands near 19 000 and 28 500 cm^{-1} are assigned, from energy considerations and their increase of intensity on cooling, to pair transitions.

The study of the optical properties of hematite and ferrites [22] may explain their photoelectrochemical properties; the relatively large absorption coefficient in the visible region due to the intensification of the spin forbidden Fe^{3+} pair transitions by antiferromagnetic couplings can account for the first process of charge carrier generation. This interpretation differs from that usually accepted [9, 31].

Acknowledgement

The authors gratefully acknowledge the International Atomic Energy Agency (contract No. 7681/RB) and National Research Foundation of Hungary (contract No. TOO 7266) for their support of this study.

References

1. S. MUSIĆ, S. POPOVIĆ and M. RISTIĆ, *J Mater. Sci.* **24** (1989) 2722.
2. *Idem, ibid.* **28** (1993) 632.
3. M. RISTIĆ, S. POPOVIĆ and S. MUSIĆ, *Mater. Lett.* **16** (1993) 309.
4. S. POPOVIĆ, M. RISTIĆ and S. MUSIĆ, *ibid.* **23** (1995) 139.
5. Powder Diffraction File, Cards no. 13-534, 6-504, 10-173. (International Centre for Diffraction Data, Newtown Square, PA, USA)
6. F. LIEBAU, "Structural Chemistry for Silicates" (Springer-Verlag, Berlin, 1985)
7. S. NAGY and T. W. WEIR, The SIRIUS Evaluating Program (The Manual for Internal Use), CSCR, Lehigh University, Bethlehem, PA, USA.
8. P. TSOKOV, V. BLASKOV, D. KLISSURSKI and I. TSOLOVSKI, *J. Mater. Sci.* **28** (1993) 184.
9. G. BUSCA, G. RAMIS, M. DEL CARMEN PRIETO and V. SANCHEZ ESCRIBANO, *J. Mater. Chem.* **3** (1993) 665.
10. S. MUSIĆ, S. POPOVIĆ, I. CZAKÓ-NAGY and S. DALIPI, *Croat. Chem. Acta* **67** (1994) 337.
11. K. VOLENIK and M. SEBERINI, *Rev. Cienc. Quim.* **14** (1983) 319.
12. J. R. SRIVASTAVA and R. P. SHARMA, *J. Physique* **35** (1974) C6-663.
13. J. K. SRIVASTAVA and S. MURALIDHARA RAO, *Phys. Stat. Sol.* (b) **90** (1978) K175.
14. B. GILLOT, F. BOUTON, F. CHASSAGNEUX and A. ROUSSET, *J. Solid State Chem.* **33** (1980) 245.
15. K. F. McCARTY and D. R. BOEHME, *ibid.* **79** (1989) 19.
16. D. M. SHERMAN and T. D. WAITE, *Amer. Miner.* **70** (1985) 1262.
17. L. A. MARUSAK, R. MESSIER and W. R. WHITE, *J. Phys. Chem. Solids* **41** (1980) 981.
18. J. FERGUSON and P. E. FIELDING, *Austr. J. Chem.* **25** (1972) 1371.
19. D. M. SHERMAN, *Phys. Chem. Miner.* **12** (1985) 161.
20. C. K. JØRGENSEN, "Oxidation Numbers and Oxidation States" (Springer-Verlag, 1969).
21. D. REINEN, *Struct. Bonding* **6** (1969) 31.
22. M. LENGLET, M. BIZI and C. K. JØRGENSEN, *J. Solid State Chem.* **86** (1990) 82.
23. M. LENGLET, unpublished results.
24. G. SMITH, *Phys. Chem. Miner.* **3** (1978) 375.
25. *Idem, Phys. Status Sol.* **61** (1980) K191
26. G. AMTHAUER and G. R. ROSSMAN, *Phys. Chem. Miner.* **11** (1984) 37.
27. D. M. SHERMAN, *ibid.* **14** (1987) 355.
28. M. LENGLET and C. K. JØRGENSEN, *Chem. Phys. Lett.* **197** (1992) 259.
29. D. S. McCLURE, *J. Chem. Phys.* **36** (1962) 2757.
30. *Idem, ibid.* **38** (1963) 2289.
31. L. G. J. de HART and G. BLASSE, *J. Electrochem. Soc.* **132** (1985) 2933.

Received 6 February 1995
and accepted 15 January 1996